Dark Energy Survey Year 1: An independent E/B-mode cosmic shear analysis

MNRAS 000, 1–6 (2018) Preprint 18 January 2019 Compiled using MNRAS LATEX style file v3.0

Dark Energy Survey Year 1: An independent E/B-mode cosmic shear analysis

Marika Asgari,[1⋆] Catherine Heymans[1]
[1]Institute for Astronomy, University of Edinburgh, Royal Observatory, Blackford Hill, Edinburgh, EH9 3HJ, U.K.

Accepted XXX. Received YYY; in original form ZZZ

ABSTRACT

We present an independent cosmic shear analysis of the non-cosmological B-mode distortions within the public first year data from the Dark Energy Survey (DES). We find no significant detection of B-modes in a full tomographic analysis of the primary METACALIBRATION shear catalogue. This is in contrast to the secondary IM3SHAPE shear catalogue, where we detect B-modes at a significance of $\sim 3\sigma$ with a pattern that is consistent with the B-mode signature of a repeating additive shear bias across the survey. We use the COSEBIs statistic to cleanly separate the B-modes from the gravitational lensing signal (E-modes). We find good agreement between the measured E-modes and their theoretical expectation given the DES cosmological parameter constraints.

Key words: Gravitational lensing: weak

1 INTRODUCTION

Cosmic shear is one of the primary cosmological probes of the large scale structures in the Universe (Bartelmann & Schneider 2001), with the potential to expand our understanding of dark matter and the accelerated expansion of the Universe. In order to release this potential we need to understand and control systematic effects that can contaminate this signal. In Asgari et al. (2018, A18 hereafter), we extracted the systematic signal from three public cosmic shear surveys, the first 450 deg^2 from the Kilo Degree Survey (KiDS-450, Hildebrandt et al. 2017), the Canada France Hawaii Telescope Lensing Survey (CFHTLenS, Heymans et al. 2012) and the Dark Energy Survey Science Verification (DES-SV, Dark Energy Survey Collaboration et al. 2016). We used COSEBIs (Complete Orthogonal Sets of E/B-Integrals, Schneider et al. 2010), which are two point statistics that cleanly separate, E-modes produced by the gravitational lensing and systematic effects from B-modes that originate from systematics only[1]. By modelling a number of terrestrial systematic effects, we showed that the choice of the statistics used for E/B-mode decomposition is important and the systematics can affect E and B-modes at different scales. The signature of the systematic effects that we modelled can be compared to the data to diagnose the origin of the B-modes.

In A18 we found evidence for systematics with a significant detection of B-mode for KiDS-450, CFHTLenS and DES-SV. We concluded the B-modes of all three surveys were consistent with a repeating additive shear bias systematic and that DES-SV, in addition, suffered from PSF-leakage and a redshift dependant selection bias. With the public release of DES first year data (Abbott et al. 2018, DES-Y1) we revisit this analysis. Zuntz et al. (2018) presented a shear power spectrum analysis of DES-Y1 concluding that the B-mode power was consistent with zero. As the main cosmological analysis of this dataset (DES Collaboration et al. 2017; Troxel et al. 2018, T18 hereafter) was carried out using the shear correlation functions, which are sensitive to different scales, we argue that this B-mode analysis is neither sufficient nor the appropriate method to then conclude zero B-mode contamination for the cosmological analysis that followed. We note that the same method was used for DES-SV which also concluded that the B-modes were insignificant in contrast to our analysis in A18 .

To quantify the effect of the systematics on the cosmological parameters, A18 employed the data compression method of Asgari & Schneider (2015), to produce compressed COSEBIs (CCOSEBIs). This method compresses the data according to its sensitivity to the parameters to be estimated. We compared the value of the measured CCOSEBIs on mock data with and without added systematics and concluded that all of the systematics that we had modelled added power to the signal. As a result the measured values of σ_8 and $\Omega_{\rm m}$ are biased high when these systematics are present in the data and thus these systematics are unable to explain the persistent tension seen between cosmological parameter constraints from weak gravitational lensing surveys and those from the cosmic microwave background (Hildebrandt et al. 2017; Troxel et al. 2018; Hikage et al. 2018; Planck Collaboration et al. 2018).

In this letter we measure COSEBIs and CCOSEBIs for DES-Y1 and compare them to the systematics modelled in A18. COSE-

⋆ E-mail: ma@roe.ac.uk

[1] Source clustering (Schneider et al. 2002) and higher order lensing effects Schneider et al. (1998) can produce currently insignificant levels of B-modes. Some of the non-standard cosmological models are also able to produce them (see for example Thomas et al. 2017).

BIs and CCOSEBIs are introduced in Section 2 and the data in Section 3. The results are shown in Section 4 and the conclusions are laid out in Section 5. Our pipeline to calculate COSEBIs is available on request.

2 METHODS

We use COSEBIs and CCOSEBIs to separate E/B-modes in DES-Y1. Here we only briefly outline the relevant equations and refer the reader to Schneider et al. (2010), Asgari & Schneider (2015) and A18 where they are introduced in more detail.

2.1 COSEBIs

COSEBIs modes can be measured from survey data using their relation to shear two point correlation functions, $\xi_\pm$,

$$E_n = \frac{1}{2}\int_{\theta_{\rm min}}^{\theta_{\rm max}} {\rm d}\theta\, \theta\, [T_{+n}(\theta)\,\xi_+(\theta) + T_{-n}(\theta)\,\xi_-(\theta)]\,, \quad (1)$$

$$B_n = \frac{1}{2}\int_{\theta_{\rm min}}^{\theta_{\rm max}} {\rm d}\theta\, \theta\, [T_{+n}(\theta)\,\xi_+(\theta) - T_{-n}(\theta)\,\xi_-(\theta)]\,, \quad (2)$$

where E_n and B_n are E and B-modes, respectively and n is a natural number, making the COSEBIs modes discrete and well-defined. The filter functions, $T_{\pm n}(\theta)$, are defined such that E_n and B_n are pure E and B-modes without a trace of ambiguous modes. As $T_{\pm n}(\theta)$ produce a complete set of basis functions, COSEBIs modes are also complete. For cosmological inference we only expect to get a signal from E_n for the first handful of n-modes (Asgari et al. 2012). This is because $\xi_\pm$ are rather smooth and featureless functions and hence their behaviour can be characterised by a small number of modes. The B_n can be used to track the remaining systematic effects, which we measure up to $n = 20$ in this analysis.

2.2 CCOSEBIs

We use the data compression method defined in Asgari & Schneider (2015) to compress COSEBIs modes to a smaller number of quantities. This compression is very useful when tomographic data is considered, especially if the analysis combines cross-correlated data from different probes, as is the current trend in cosmology. Asgari & Schneider (2015) data compression relies on the sensitivity of the data vector to the model parameters. This sensitivity is quantified by the first and second order derivatives of the observable statistics to the parameters, as well as the covariance matrix of the statistics. The addition of the second order derivatives ensures that this data compression is less prone to losing information if the covariance matrix or the derivatives are not accurate. We call the compressed COSEBIs, CCOSEBIs, which are defined as,

$$\boldsymbol{E}^{\rm c} = \boldsymbol{\Gamma}\boldsymbol{E} \quad \text{and} \quad \boldsymbol{B}^{c} = \boldsymbol{\Gamma}\boldsymbol{B}\,, \quad (3)$$

where $\boldsymbol{\Gamma}$ is the compression matrix, $\boldsymbol{E}^{\rm c}$ and $\boldsymbol{B}^{\rm c}$ are the E and B-mode CCOSEBIs, while $\boldsymbol{E}$ and $\boldsymbol{B}$ are the COSEBIs E and B-mode vectors. For $n_{\rm p}$ free parameters in the model and $N_{\rm tot}$ COSEBIs modes, $\boldsymbol{\Gamma}$ is an $n_{\rm p}(n_{\rm p}+3)/2 \times N_{\rm tot}$ matrix. The first $n_{\rm p}$ rows of $\boldsymbol{\Gamma}$ consist of the first order derivatives of E_n with respect to the parameters multiplied by their inverse covariance matrix, while the rest of the rows correspond to the second order compressed modes, formed of the second order derivatives of E_n multiplied by their inverse covariance matrix.

The cosmic shear cosmological information is contained in the E-modes and the first few COSEBIs modes capture this information. Therefore, the CCOSEBIs modes are formed of these modes. Here we only consider σ_8 and $\Omega_{\rm m}$ as free parameters and form the CCOSEBIs for these parameters, resulting in five CCOSEBIs modes, two first order modes: $E^{\rm c}_{\sigma_8}$ and $E^{\rm c}_{\Omega_{\rm m}}$ and three second order modes: $E^{\rm c}_{\sigma_8\sigma_8}$, $E^{\rm c}_{\sigma_8\Omega_{\rm m}}$ and $E^{\rm c}_{\Omega_{\rm m}\Omega_{\rm m}}$. This reduction in data volume can be compared to the 200 COSEBIs modes considered for a 4 tomographic bin analysis with 10 redshift bin pair combinations and $n = 20$ mode measurements for each.

3 DATA ANALYSIS

The first year data release of the Dark Energy Survey[2] (DES-Y1, Abbott et al. 2018) consists of 1514 deg^2 of cosmic shear data in four photometric bands $griz$ (see Morganson et al. 2018; Flaugher et al. 2015, for the image processing pipeline and the camera specifications). This data has been analysed with two distinct shape measurement methods: IM3SHAPE and METACALIBRATION (Zuntz et al. 2018). METACALIBRATION is a method that calibrates the results of any shape measurement method based on its sensitivity to shearing the image in different directions. For DES-Y1, METACALIBRATION is applied to shape measurements from a Gaussian model that is fit to the light profile of the galaxies as imaged in the riz photometric bands, resulting in ellipticity measurements for ~ 31 million galaxies. This is the primary catalogue for the cosmic shear analysis presented in T18 and DES Collaboration et al. (2017), both of which use a subset of this catalogue that overlaps with their REDMAGIC galaxy sample, resulting in a reduced area of 1321 deg^2. IM3SHAPE is a model fitting method that uses image simulations for calibration (Samuroff et al. 2018). For the DES-Y1 analysis, IM3SHAPE in contrast to METACALIBRATION analyses the r-band only, yielding a lower signal-to-noise catalogue with ~ 21 million galaxies. This catalogue was primarily used for consistency checks. Here we show results for both catalogues for the full available area.

T18 measured correlation functions between $\theta \in [2.5', 250']$, but used a variable minimum angular distance for their cosmological analysis, to avoid sensitivity to baryonic feedback (Semboloni et al. 2011). They used either $\theta_{\rm min} = 4'$ or $\theta_{\rm min} = 8'$ for ξ_+ and $\theta_{\rm min} = 40'$ or $\theta_{\rm min} = 100'$ for ξ_-, keeping $\theta_{\rm max} = 250'$ in all cases. In this paper we analyse these five angular ranges: $[0.5', 250']$, $[4', 250']$, $[8', 250']$, $[40', 250']$ and $[100', 250']$, which cover all ranges analysed by T18 with the addition of a larger angular range, $[0.5', 250']$, anticipating future analyses that may use smaller scales (see for example MacCrann et al. 2017). Following T18 we divide the data into four photometric-redshift bins: $z_{\rm phot} \in (0.2, 0.43)$, $z_{\rm phot} \in (0.43, 0.63)$, $z_{\rm phot} \in (0.63, 0.9)$, $z_{\rm phot} \in (0.9, 1.3)$ and also include a combined bin of $z_{\rm phot} \in (0.2, 1.3)$. We show predictions for the E-modes using the best fitting cosmological and nuisance parameters assuming a flat-ΛCDM model based on the cosmic shear only analysis of T18 (see Table 1) and the redshift distributions described in Hoyle et al. (2018). The theory predictions are calculated with COSMOSIS (Zuntz et al. 2015)[3] using the setup adopted by T18 : CAMB for the linear matter power spectrum (Lewis et al. 2000; Howlett et al. 2012)[4], Takahashi et al. (2012) for the nonlinear evolution

[2] https://des.ncsa.illinois.edu/releases/y1a1
[3] COSMOSIS: bitbucket.org/joezuntz/cosmosis
[4] CAMB: http://camb.info

Table 1. The best-fitting cosmological parameters for DES-Y1 METACALIBRATION (Mcal) and IM3SHAPE (Im3) catalogues (T18), estimated from their cosmological chains. σ_8 is the standard deviation of perturbations in a sphere of radius $8h^{-1}\mathrm{Mpc}$, today. n_s is the spectral index of the primordial power spectrum. Ω_m, Ω_b and Ω_ν are the matter, baryon and neutrino density parameters, respectively and h is the dimensionless Hubble parameter. The underlying cosmology is a flat-ΛCDM model with Gaussian initial perturbations. The last two columns show the intrinsic alignment parameters: A_IA, the amplitude of the intrinsic galaxy alignment model and η characterising the redshift dependence of the intrinsic alignments around a pivot redshift of $z_0 = 0.62$.

	σ_8	Ω_m	n_s	h	Ω_b	Ω_ν	A_IA	η
Mcal	0.81	0.29	0.97	0.74	0.033	0.010	1.40	1.43
Im3	0.63	0.48	0.92	0.62	0.031	0.016	0.48	-0.41

of matter, Bridle & King (2007)[5] for the intrinsic alignments with an additional redshift dependence characterised by a power and a pivot redshift (see Table 1). In addition, we include the four multiplicative shear calibration parameters as well as another four additive photometric redshift bias parameters in our predictions. For the single bin theory predictions we set the nuisance parameters to zero and find that this provides a good fit to the non-tomographic data.

To calculate COSEBIs we measure 2PCFs using ATHENA[6] (Kilbinger et al. 2014) with a million linear angular bins in $[0.5', 250']$. See Asgari et al. (2017) for a series of accuracy tests when measuring COSEBIs.

4 RESULTS

We present COSEBIs and CCOSEBIs measurements for both IM3SHAPE and METACALIBRATION catalogues, focusing on the significance of the measured B-modes. To do so we measure p-values for the B-modes given a null model with a Gaussian distribution. A p-value shows the probability of measuring a B-mode signal that is equally or more extreme than the one measured from the data, given the model (see Appendix C of A18 for more details). To calculate the p-values we need to first calculate the χ^2 values for which a covariance matrix is needed. In the absence of systematics or physical phenomena that can produce B-modes, this covariance matrix will only depend on the weighted number of galaxy pairs, N_pair, and the weighted dispersion in galaxy shapes, σ_ϵ [7]. We use the measured N_pair and σ_ϵ from the data to form the covariance matrix. When comparing the E-modes to their expectation values based on the T18 best-fit parameters in Table 1, we add the cosmic variance terms to the Gaussian covariance but ignore the sub-dominant non-Gaussian and super sample terms.

The covariance matrix for the CCOSEBIs can be derived from the COSEBIs covariance, by multiplying both sides with the compression matrix, $\mathbf{\Gamma}$. More details about the covariance calculation is given in the method section of A18.

We first look at the COSEBIs measurements for a non-tomographic analysis in Fig. 1 showing results for METACALIBRATION (blue squares) and IM3SHAPE (black circles). Here we only show results for the $[4', 250']$ angular range, that corresponds to the widest angular range used in T18. On the left hand side we show E-modes and on the right B-modes finding the B-modes for METACALIBRATION to be consistent with zero. In contrast, the IM3SHAPE E/B-modes show unexpected oscillations that resemble the systematic signature of a repeating additive shear bias (see figure 10 in A18). This feature was also apparent in the DES-SV COSEBIs analysis (A18).

Table 2. B-mode p-values for the METACALIBRATION catalogue. Each row shows a different angular separation range. The first two columns of numbers show p-values for COSEBIs with 20 modes and the last two columns belong to compressed COSEBIs. All p-values smaller than 0.01, corresponding to 2.3 σ, are shown in boldface. The results are shown for both tomographic and non-tomographic cases.

	COSEBIs		CCOSEBIs	
θ range	Single Bin	Tomo	Single Bin	Tomo
$[0.5', 250']$	0.16	0.11	0.20	0.07
$[4', 250']$	0.33	0.35	0.88	0.96
$[8', 250']$	0.67	0.10	0.34	0.64
$[40', 250']$	0.80	0.17	0.91	0.78
$[100', 250']$	0.46	0.03	0.76	0.25

In Fig. 2 we present the CCOSEBIs analysis for the non-tomographic (left) and tomographic (right) cases. The blue symbols and curves represent METACALIBRATION (squares: E-modes and circles: B-modes) and the black symbols and the dashed curve represent IM3SHAPE (right facing triangles: E-modes and left facing triangles: B-modes). The angular range used here is the same as in Fig. 1, with $\theta \in [4', 250']$. The E-modes match their predicted theory values well. CCOSEBIs for σ_8 and Ω_m are highly correlated and we caution the reader if carrying out a visual inspection.

We summarise our analysis for the other angular ranges in the form of p-values for the B-modes in Tables 2, 3, 4 and 5. All p-values < 0.01 are shown as bold ($> 2.3\sigma$ detection). Tables 2 and 3 show p-values for the COSEBIs and CCOSEBIs B-mode measurements for 5 angular ranges and for the single bin and tomographic cases. In Table 2 we show results for METACALIBRATION, while in Table 3 IM3SHAPE results are shown. We see that the p-values show no significant B-modes for the primary METACALIBRATION DES-Y1 shape catalogues, for all angular ranges. This is, however, not the case for the IM3SHAPE results, where, there is a detection of COSEBIs B-modes in the $[0.5', 250']$ angular range for both tomographic (3.4σ) and non-tomographic (2.3σ) cases as well as the tomographic case for $[4', 250']$ (2.8σ). The CCOSEBIs results which are not sensitive to higher COSEBIs modes do not show any significant B-modes, however as we have shown in A18, this does not guarantee that the E-modes are not affected by these systematics, since some systematic effects, such as a repeating bias pattern have a different signature for E and B-modes. For these systematics even though they affect higher order B-modes more significantly, they tend to produce E-modes for the lower COSEBIs modes. As a result they will bias the cosmological analysis.

χ^2 is a quantity that compresses all the information into a single summary statistic and takes a weighted average over the data, therefore, it is not always the most informative quantity. As a result, in Tables 4 and 5 we separately analyse the auto and cross-correlations in the tomographic data for the different redshift bin pairs and calculate p-values for COSEBIs in each case. Table 4 shows results for METACALIBRATION and Table 5 for IM3SHAPE. Here we see that the significant B-modes detected for IM3SHAPE do not result in a significant p-value for any of the redshift bin pairs individually, but as many of these p-values are close to the

[5] `bk_corrected` in COSMOSIS
[6] ATHENA: www.cosmostat.org/software/athena
[7] This analytical result is validated against simulations in Asgari et al. (2017).

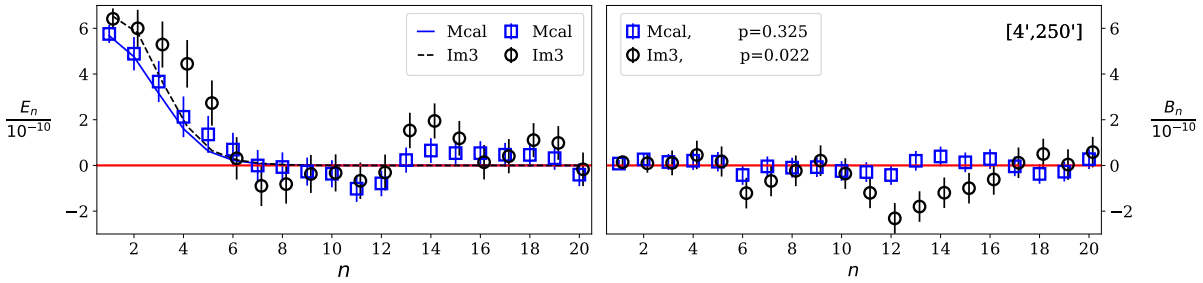

Figure 1. COSEBIs E-modes (left) and B-modes (right) for DES-Y1 catalogues. METACALIBRATION results are shown in blue and IM3SHAPE in black. The p-values shown in the legends correspond to the B-modes assuming a null hypothesis of zero B-modes. The angular range considered here is $[4', 250']$. Note that COSEBIs modes are discrete and the theory values are connected to each other only for visual aid. The errors for E-modes include cosmic variance terms and hence are larger than the B-mode errorbars.

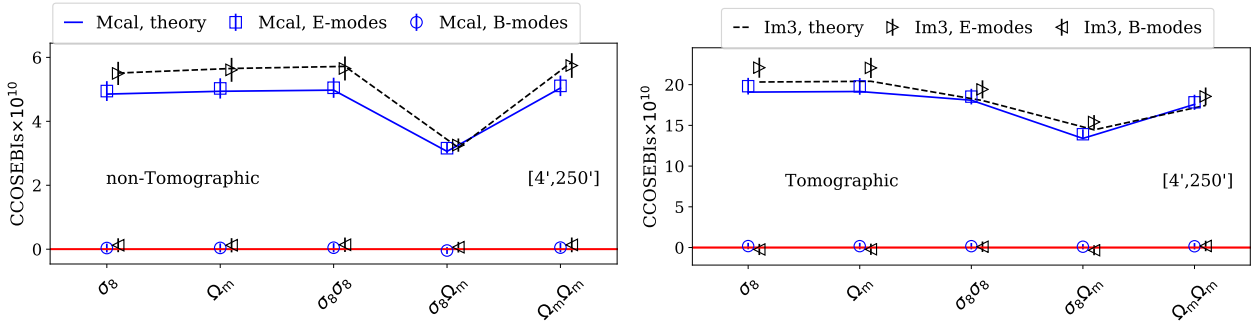

Figure 2. Compressed COSEBIs results for METACALIBRATION (blue) and IM3SHAPE (black) catalogues. The angular separation range is $[4', 250']$ and the results are shown for non-tomographic (left) and tomographic (right) cases. B-modes are shown to be consistent with zero for both catalogues. The expected theory values for E-modes are shown as curves (see Table 1 for the input cosmological parameters). Note that CCOSEBIs modes are discrete and the theory values are connected to each other only for visual aid.

Table 3. Same as Table 2, but for IM3SHAPE catalogues.

	COSEBIs		CCOSEBIs	
θ range	Single Bin	Tomo	Single Bin	Tomo
$[0.5', 250']$	$\mathbf{9.8e-3}$	$\mathbf{3.7e-4}$	0.23	0.07
$[4', 250']$	0.02	$\mathbf{2.2e-3}$	0.89	0.44
$[8', 250']$	0.06	0.01	0.17	0.22
$[40', 250']$	0.10	0.06	0.30	0.89
$[100', 250']$	0.11	0.03	0.19	0.87

threshold, their "averaged" p-value becomes significant. On the other hand we see that although none of the METACALIBRATION p-values were significant in Table 2, the combination of the two highest redshift bins, z-34, shows significant B-modes of up to 3.0σ for 3 of the angular ranges. On inspection, the B-mode in the z-34 bin combination has oscillatory features out to high n-modes, similar to the pattern expected from a repeating additive shear bias. When all the bins are combined, however, this significant detection is cancelled by the large p-values for the lower redshift bins. The distribution of the METACALIBRATION p-values in Table 4 is essentially flat which is expected if the model (zero B-modes) is a good description of the data. The distribution of the IM3SHAPE p-values in Table 5, however, shows a visible skewness towards smaller values which indicates that the zero B-mode model is a poor fit (see Appendix C in A18).

Table 4. B-mode p-values for METACALIBRATION catalogues split for each pair of redshift bins. Each row presents p-values for the given redshift bin pair, z-ij, corresponding to the COSEBIs measured for redshift bins i and j. The results are shown for 5 angular ranges and 20 COSEBIs modes. The boldfaced values correspond to p-value < 0.01 and hence a significant B-mode detection, larger than 2.3 σ.

	$[0.5', 250']$	$[4', 250']$	$[8', 250']$	$[40', 250']$	$[100', 250']$
z-11	1.00	1.00	0.99	0.86	0.60
z-12	0.84	0.90	0.59	0.80	0.68
z-13	0.49	0.41	0.67	0.43	0.69
z-14	0.48	0.35	0.77	0.60	0.75
z-22	0.04	0.12	0.11	0.85	0.38
z-23	0.18	0.63	0.48	0.95	0.52
z-24	0.13	0.07	0.03	0.03	0.22
z-33	0.06	0.41	0.16	0.11	0.15
z-34	0.09	0.03	$\mathbf{1.2e-3}$	$\mathbf{2.1e-3}$	$\mathbf{1.6e-3}$
z-44	0.51	0.71	0.79	0.22	0.01

5 CONCLUSIONS

One of the major challenges for current and future cosmic shear analysis is the appropriate treatment of systematic effects. With COSEBIs we can separate E/B-modes completely and efficiently.

Table 5. Same as Table 4 but for IM3SHAPE catalogues.

	$[0.5', 250']$	$[4', 250']$	$[8', 250']$	$[40', 250']$	$[100', 250']$
z-11	0.03	0.03	0.04	0.54	0.35
z-12	0.03	0.03	0.29	0.16	0.04
z-13	0.43	0.92	0.80	0.58	0.21
z-14	0.11	0.02	0.06	0.05	0.03
z-22	0.29	0.47	0.43	0.60	0.36
z-23	0.19	0.49	0.26	0.79	0.89
z-24	0.25	0.25	0.23	0.05	0.28
z-33	0.10	0.08	0.05	0.33	0.49
z-34	0.20	0.10	0.34	0.21	0.22
z-44	0.03	0.17	0.19	0.16	0.19

The B-modes of COSEBIs are very sensitive to the systematic effects in the data and can be used as a diagnosis tool. In addition, its E-modes can be used for cosmological analysis, allowing for a consistent treatment of the data for both E and B-modes. Here we followed the analysis of Asgari et al. (2018) measuring COSEBIs and CCOSEBIs E/B-modes for both catalogues of the DES-Y1 data. We found that METACALIBRATION has B-modes that are consistent with zero for the full tomographic analysis. On inspection of individual bin combinations, however, we found the z-34 bin to be an outlier with a 3.0σ B-mode. This low-level B-mode from a single bin is unexpected to produce any biases in the cosmological analysis for the current volume of the data. For future data releases, however, this signal should be investigated further as the last redshift bins have the highest signal-to-noise contribution to the cosmological analysis.

A tomographic analysis of the IM3SHAPE catalogue shows a significant detection of B-modes up to 3.4σ. Although IM3SHAPE is not used in the primary DES cosmological analysis it is used for validation. If the B-modes in the IM3SHAPE catalogues persist, their use as a validation tool becomes limited.

Hildebrandt et al. (2018) presents an updated cosmic shear analysis of the Kilo-Degree Survey (KiDS) that incorporates near infra-red photometry (Wright et al. 2018) and a number of other improvements (Kannawadi et al. 2018). They conclude that their control of systematics has significantly improved in this new 9-band analysis, with the previously reported significant B-mode detection found to now be consistent with zero. Given this development for KiDS, and our independent verification of the high quality systematic control within DES, we see a very promising future for high accuracy cosmic shear cosmology.

ACKNOWLEDGEMENTS

We thank Ami Choi, Niall MacCrann, Michael Troxel and Joe Zuntz for their help with using the DES-Y1 products and useful discussions. We thank Vasiliy Demchenko and the referee for useful comments. We acknowledge support from the European Research Council (grant number 647112).

This project used public archival data from the Dark Energy Survey (DES). Funding for the DES Projects has been provided by the U.S. Department of Energy, the U.S. National Science Foundation, the Ministry of Science and Education of Spain, the Science and Technology Facilities Council of the United Kingdom, the Higher Education Funding Council for England, the National Center for Supercomputing Applications at the University of Illinois at Urbana–Champaign, the Kavli Institute of Cosmological Physics at the University of Chicago, the Center for Cosmology and Astro-Particle Physics at the Ohio State University, the Mitchell Institute for Fundamental Physics and Astronomy at Texas A&M University, Financiadora de Estudos e Projetos, Fundação Carlos Chagas Filho de Amparo à Pesquisa do Estado do Rio de Janeiro, Conselho Nacional de Desenvolvimento Científico e Tecnológico and the Ministério da Ciência, Tecnologia e Inovação, the Deutsche Forschungsgemeinschaft, and the Collaborating Institutions in the Dark Energy Survey. The Collaborating Institutions are Argonne National Laboratory, the University of California at Santa Cruz, the University of Cambridge, Centro de Investigaciones Energéticas, Medioambientales y Tecnológicas-Madrid, the University of Chicago, University College London, the DES-Brazil Consortium, the University of Edinburgh, the Eidgenössische Technische Hochschule (ETH) Zürich, Fermi National Accelerator Laboratory, the University of Illinois at Urbana-Champaign, the Institut de Ciències de l'Espai (IEEC/CSIC), the Institut de Física d'Altes Energies, Lawrence Berkeley National Laboratory, the Ludwig-Maximilians Universität München and the associated Excellence Cluster Universe, the University of Michigan, the National Optical Astronomy Observatory, the University of Nottingham, The Ohio State University, the OzDES Membership Consortium, the University of Pennsylvania, the University of Portsmouth, SLAC National Accelerator Laboratory, Stanford University, the University of Sussex, and Texas A&M University. Based in part on observations at Cerro Tololo Inter-American Observatory, National Optical Astronomy Observatory, which is operated by the Association of Universities for Research in Astronomy (AURA) under a cooperative agreement with the National Science Foundation.

REFERENCES

Abbott T. M. C., et al., 2018, preprint, (arXiv:1801.03181)
Asgari M., Schneider P., 2015, A&A, 578, A50
Asgari M., Schneider P., Simon P., 2012, A&A, 542, A122
Asgari M., Heymans C., Blake C., Harnois-Deraps J., Schneider P., Van Waerbeke L., 2017, MNRAS, 464, 1676
Asgari M., et al., 2018, preprint, (arXiv:1810.02353)
Bartelmann M., Schneider P., 2001, Phys. Rep., 340, 291
Bridle S., King L., 2007, New Journal of Physics, 9, 444
DES Collaboration et al., 2017, preprint, (arXiv:1708.01530)
Dark Energy Survey Collaboration et al., 2016, MNRAS, 460, 1270
Flaugher B., et al., 2015, AJ, 150, 150
Heymans C., et al., 2012, MNRAS, 427, 146
Hikage C., et al., 2018, preprint, (arXiv:1809.09148)
Hildebrandt H., et al., 2017, MNRAS, 465, 1454
Hildebrandt H., et al., 2018, arXiv e-prints,
Howlett C., Lewis A., Hall A., Challinor A., 2012, J. Cosmology Astropart. Phys., 4, 027
Hoyle B., et al., 2018, MNRAS, 478, 592
Kannawadi A., et al., 2018, arXiv e-prints,
Kilbinger M., Bonnett C., Coupon J., 2014, athena: Tree code for second-order correlation functions, Astrophysics Source Code Library (ascl:1402.026)
Lewis A., Challinor A., Lasenby A., 2000, ApJ, 538, 473
MacCrann N., et al., 2017, MNRAS, 465, 2567
Morganson E., et al., 2018, PASP, 130, 074501
Planck Collaboration et al., 2018, preprint, (arXiv:1807.06209)
Samuroff S., et al., 2018, MNRAS, 475, 4524
Schneider P., van Waerbeke L., Jain B., Kruse G., 1998, MNRAS, 296, 873
Schneider P., van Waerbeke L., Mellier Y., 2002, A&A, 389, 729
Schneider P., Eifler T., Krause E., 2010, A&A, 520, A116
Semboloni E., Hoekstra H., Schaye J., van Daalen M. P., McCarthy I. G., 2011, MNRAS, 417, 2020
Takahashi R., Sato M., Nishimichi T., Taruya A., Oguri M., 2012, ApJ, 761, 152
Thomas D. B., Whittaker L., Camera S., Brown M. L., 2017, MNRAS, 470, 3131
Troxel M. A., et al., 2018, Phys. Rev. D, 98, 043528
Wright A. H., et al., 2018, arXiv e-prints,
Zuntz J., et al., 2015, Astronomy and Computing, 12, 45
Zuntz J., et al., 2018, MNRAS, 481, 1149

This paper has been typeset from a TEX/LATEX file prepared by the author.